



# Numerical Simulation of Flow around a High-Speed Train Subjected to Different Windbreak Walls and Yaw Angles

J. Zhang, K. He, J. Wang, T. Liu, X. Liang and G. Gao<sup>†</sup>

*Key Laboratory of Traffic Safety on Track of Ministry of Education, School of Traffic & Transportation Engineering, Central South University, Changsha 410075, China*  
*Joint International Research Laboratory of Key Technology for Rail Traffic Safety, Central South University, Changsha 410075, China*  
*National & Local Joint Engineering Research Center of Safety Technology for Rail Vehicle, Changsha 410075, China*

<sup>†</sup>Corresponding Author Email: [gjgao@csu.edu.cn](mailto:gjgao@csu.edu.cn)

(Received July 30, 2018; accepted October 24, 2018)

## ABSTRACT

The prediction of flow around a high-speed train subjected to different windbreak walls and yaw angles has been investigated using steady Shear Stress Transport (SST)  $k-\omega$  turbulence model at the Reynolds number of  $1.0 \times 10^6$  based on the height of the scaled train model. The results show that an effective windbreak wall provide a favourable shielding effect for the train behind it, and force the primary positive pressure on the windward of the train to transfer on the wall. Consequently, the airflow cannot directly act on the train body, and the train is basically in an environment with small negative pressure. The inclined slope (the earth embankment type) windbreak wall shows poor anti-wind performance that should not be used along the new high-speed railways. When designing the windbreak wall, the influences of yaw angles should be taken into account.

**Keywords:** High-speed train; Windbreak wall; Yaw angle; Crosswind; Numerical simulation.

## NOMENCLATURE

$A$	reference area	$P$	static pressure
$C_p$	pressure coefficient	$P_{ref}$	reference pressure
$C_l$	lift force coefficient	$q$	dynamic pressure
$C_s$	side force coefficient	$U$	upstream velocity
$C_M$	overturning moment coefficient	$v_t$	train speed
$F_s$	side force	$v_w$	crosswind speed
$F_l$	lift force		
$h$	reference height	$\rho$	air density
$k$	turbulence kinetic energy	$\omega$	specific dissipation rate
$M$	overturning moment		

## 1. INTRODUCTION

With rapid development of faster and lighter high-speed trains in the last decades, crosswind stability has become one of the most attracting issues in train aerodynamics. The flow around a train subjected to crosswinds is characterized by large separation from the leeward of the head car and the inter-carriage gaps, and the presence of trailing vortices, as shown in Khier *et al.* (2000), Hemida and Krajnovic (2010), Yao *et al.* (2014) and Zhang *et*

*al.* (2017a), which has great effects on the operational safety of the train and lowers the running stability with an increasing risk of overturning. Consequently, in China, 38 accidents are estimated to have been caused by strong winds until 2009 (Ge *et al.*, 2009). In Japan, 29 such accidents have been reported before 2003 (Suzuki *et al.*, 2003). In European, Oceanian, North and South American countries, there are also serious railway accidents caused by crosswinds (Wikipedia 2015; Peters, 2004; Rolén, 2004; Wetzels and Proppe, 2007).

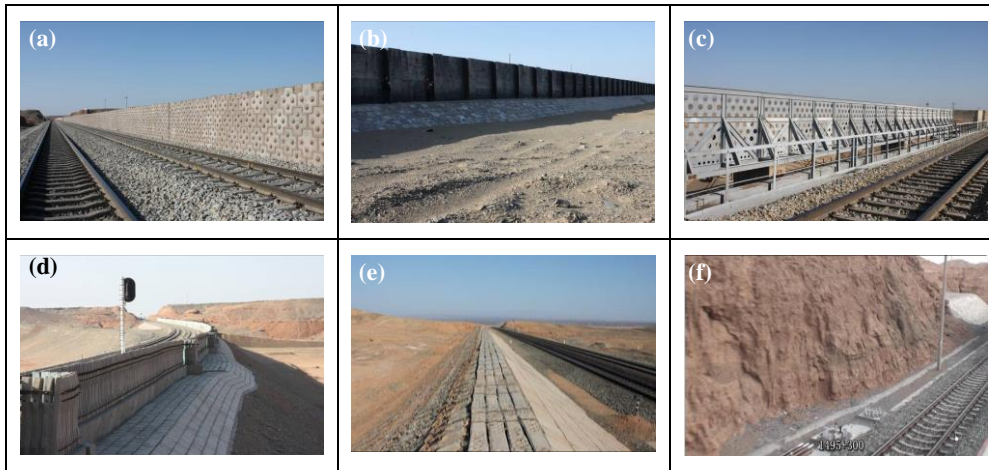


**Fig. 1. Windbreak facilities: (a) Reinforcement type, (b) Concrete type, (c) Bridge type with holes, (d) Concrete tie with plate type, (e) Earth embankment type, (f) Cut.**

These incidents caused massive damage and economic loss. Therefore, it is necessary to take measures to reduce the effects of crosswinds on the trains.

According to previous work, all those measures can be summarized as: (1) Aerodynamic optimization of train shapes (Cheli, 2010; Hemida and Krajnovic, 2010; Zhang *et al.*, 2011; Chen *et al.*, 2018), (2) Regulation of train operation (Fujii *et al.*, 1999; Gong and Wang, 2012; Liu *et al.*, 2009; Gao *et al.*, 2015; Zhang *et al.*, 2015a and 2016), and (3) Construction of efficient windbreak facilities (Fujii *et al.*, 1999; Baker, 1999; Bocciolone, *et al.*, 2008; Tomasini *et al.*, 2016; Zhang and Liu, 2012 and 2014; Zhang *et al.*, 2013 and 2017b).

From the view of train operational safety and railway transportation efficiency, windbreak facilities have been proven to be one of the most economic and practical approaches. In Europe and Japan, as the main windbreak facilities, straight windbreak walls with very thin thickness and uniform porosity that are made of perforated steel sheets are used widely, and their windbreak performance has been investigated (Baker, 1999; Fujii *et al.*, 1999; Tomasini *et al.*, 2016; Avila-Sanchez *et al.*, 2016). While in Xinjiang of China, due to the complex wind conditions (Ge *et al.*, 2009), the trains run on the Xinjiang railway lines would be subjected to the desert wind, so the walls with porosity, except of these on the high bridges, will not be a good choice. Five walls (Zhang *et al.*, 2017b) and one cut (Liu and Zhang, 2013; Zhang *et al.*, 2015b) that are usually built using local material can be found, i.e. the earth embankment type, reinforcement type, concrete tie with plate type, concrete type and bridge type with holes, see Fig. 1. As a result, Xinjiang has become an exhibition centre of windbreak facilities as compared to other regions around the world. As indicated in Zhang *et al.* (2017b), different windward sides of the windbreak walls show different anti-wind performances. Therefore, there is a need for a study that investigates the aerodynamic properties of high-speed trains subjected to different windbreak

walls in order to understand the flow around the trains behind windbreak walls and determine the type of windbreak walls along reconstructive electrified railways. Additionally, since the wind is not always normal to the railways and its speed is variable, yaw cases are often taken into account to explore the combination effect of train speed and wind speed on the aerodynamic performance of the train without windbreaks, as seen in (Khier *et al.*, 2000; Hemida and Krajnovic, 2010; Rezvani and Mohebbi, 2014; Sima *et al.*, 2015; Avadiar *et al.*, 2016). Although some wind tunnel tests on the yaw effects were carried out with straight porous windbreak walls (Baker, 1999; Bocciolone *et al.*, 2008; Tomasini *et al.*, 2016), few studies have been conducted on those windbreak walls that are used for high-speed trains on the Xinjiang railways. The reinforcement type, concrete type and concrete tie with plate type are all straight walls only with different thicknesses in the spanwise direction. They have similar shielding effects for the train according to previous study (Zhang and Liu, 2014). As to the cut, related work has been conducted in Liu and Zhang (2013) and Zhang *et al.* (2015b). Therefore, in this study, three different types of windbreak walls, i.e. straight solid (the reinforcement type), inclined slope (the earth embankment type) and bridge windbreak walls were used to simulate the flow field distribution around the train subjected to different windbreak walls and yaw angles.

## 2. NUMERICAL SET-UP AND VALIDATION

### 2.1 Computational Details

The detailed information about the high-speed train model can be found in previous work (Zhang *et al.*, 2017a). Here, three different types of windbreak walls, i.e. straight solid (the reinforcement type) (SSWW), inclined slope (the earth embankment type) (ISWW) and bridge (BWW) windbreak walls are shown in Fig. 2. The height of the walls is 3 m, and the porosity of the bridge type is 30%. Figure 3

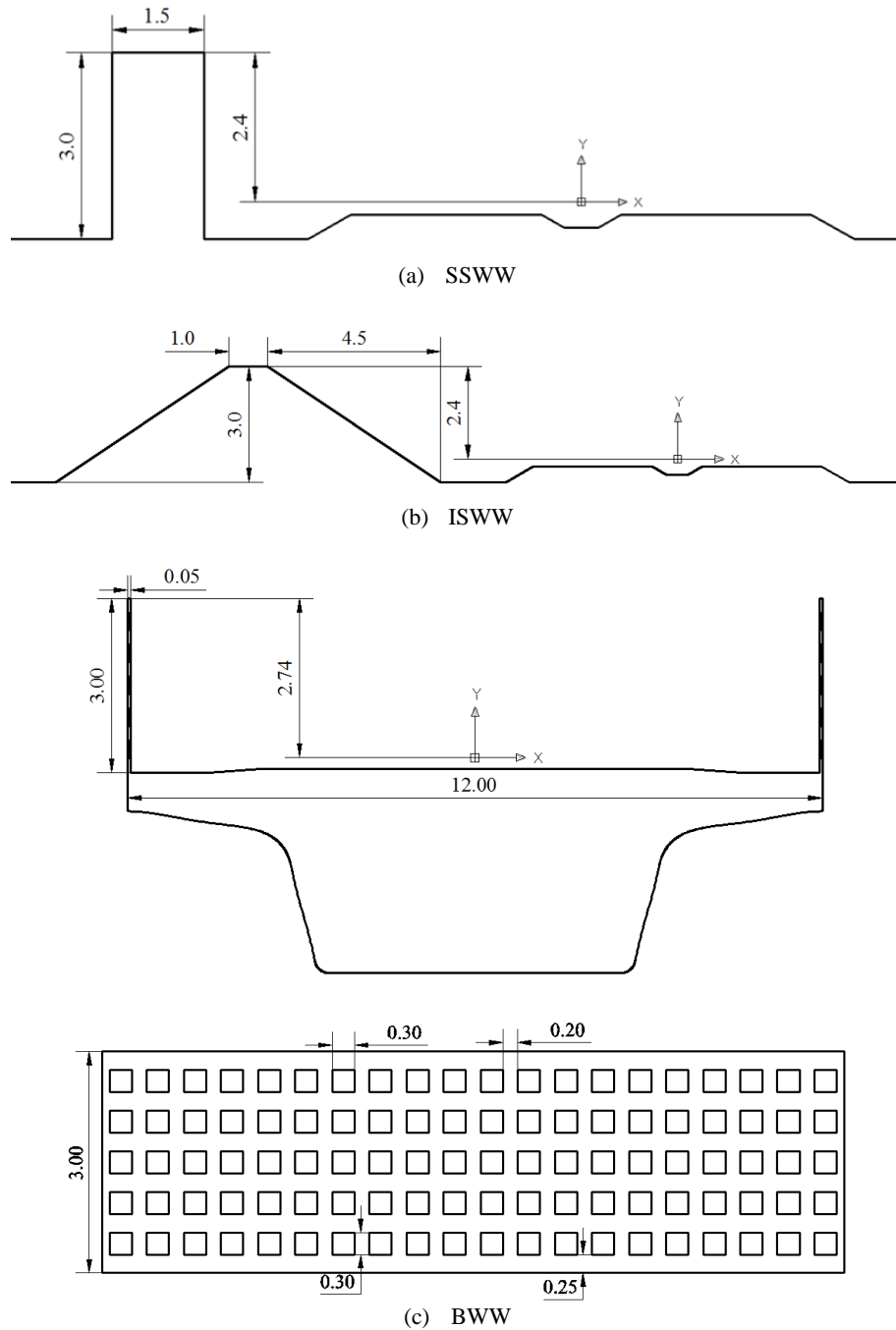


**Fig. 2.** Cross sections of different types of windbreak walls (unit: m).

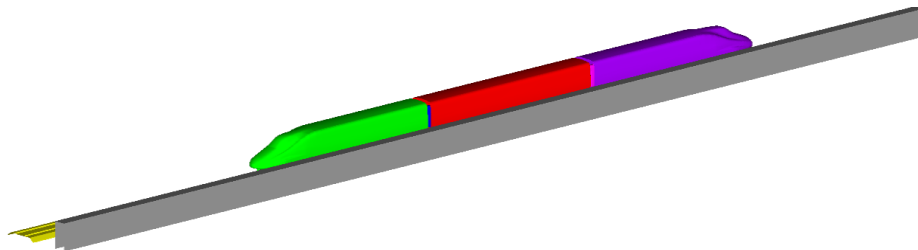


**Fig. 3.** Computational model.

shows the relative location between the train and the windbreak wall. In this paper, the computational domain and boundary conditions are the same as

those used in the related study (Zhang *et al.*, 2017a). So to reduce the repetition, this part will not be listed here.

The mesh strategy used is also highly similar to that was used in Zhang *et al.* (2017a). However, as a windbreak was added in the domain, the refinement box has been enlarged to enclose the train, the ballast and the wall. Thus, to reduce the repetition, mesh distributions only focus on train-windbreak surfaces, as show in Fig. 4.

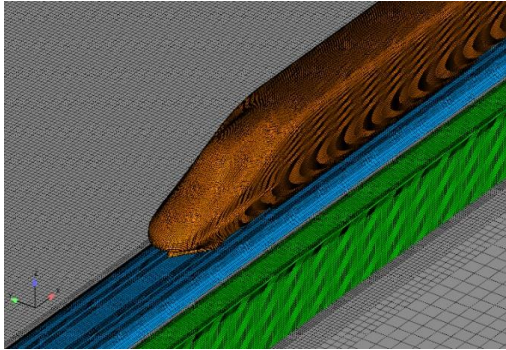


**Fig. 4. Grid distributions on train-windbreak wall surfaces.**

In this paper, the commercial CFD software ANSYS Fluent was used, and the Finite Volume Method (FVM) based on cell centres was adopted for the discretization of the controlling equations. Simulations were performed using a pressure-based solver. A second-order upwind scheme was chosen to solve the momentum,  $k$  and  $\omega$  equations. The SIMPLEC (Semi-Implicit Method for Pressure-Linked Equations-Consistent) algorithm was used in the computational method to couple the pressure and the velocity field. The convergence criterion was based on the residual value of the continuity equation being set at  $10^{-6}$  with minimal fluctuation. The convergence was also monitored by plotting the aerodynamic force coefficients on the middle car until the variation of the force became steady with iterations.

For the convenience of comparative analysis, the non-dimension coefficients are defined as follows.

$$C_s = F_s / (qA), C_l = F_l / (qA), C_M = M / (qAh) \quad (1)$$

$$C_p = (P - P_{ref}) / q \quad (2)$$

Where,  $q=0.5\rho U^2$ ,  $q$  is the dynamic pressure.  $U$  is the upstream velocity.  $F_s$ ,  $F_l$  and  $M$  are the side force, lift force and overturning moment respectively, corresponding to the coefficients  $C_s$ ,  $C_l$  and  $C_M$ .  $A$  is the reference area which is  $0.0556 \text{ m}^2$  in analysis.  $h$  is  $0.225 \text{ m}$ .  $\rho$  is the constant air density that is  $1.177 \text{ kg/m}^3$ .  $C_p$  is the pressure coefficient.  $P$  is the static pressure on train body.  $P_{ref}$  is the reference pressure of 0.

## 2.2 Validation

In this paper, the steady Shear Stress Transport (SST)  $k-\omega$  turbulence model that has been widely used in train aerodynamics was used to simulate the flow around the train-windbreak wall. Since there is a wall included in the present study, it is better that

a comparison is made between those numerical and experimental data with the windbreak wall, but unfortunately, no wind tunnel test concerning the same train-windbreak wall model has been conducted. In the previous study (Zhang *et al.*, 2017a), the numerical method was validated against wind tunnel experiments without windbreak walls, and good agreement was shown for the overturning moment coefficients  $C_M$  within errors of less than 6%. The experiments were conducted in the test section of the wind tunnel in the Low Speed Aerodynamic Institute of China Aerodynamics Research & Development Center (CARD). The cross-sectional area of the tunnel in the test section is  $8 \times 6 \text{ m}^2$ . To decrease the thickness of boundary layers, a fixed ground board mounted on a turntable was installed. A  $1/15^{\text{th}}$ -scale train model consisted of three cars was placed on the flat ground board with the incoming flow speed set at  $60 \text{ m/s}$ . In general, it can assume the numerical method and simulation settings are appropriate for the train-windbreak case in the present study.

## 3. RESULTS AND DISCUSSION

In this section, the influences of windbreak walls and yaw angles on the crosswind performance of the train are investigated by the 3D streamlines, pressure distributions and aerodynamic forces.

### 3.1 Different Windbreak Walls

Currently, those windbreak walls in Xinjiang of China can be listed as 3 typical categories: Straight solid (the reinforcement type) (SSWW), inclined slope (the earth embankment type) (ISWW) and bridge (BWW) windbreak walls. The flow fields around the train-windbreak wall are different when the train runs behind different windbreak walls. In order to investigate those differences on the flow structures, the steady Reynolds-averaged Navier–Stokes (RANS) was used to simulate the train running behind the windbreak walls, and the aerodynamic characteristics were also analysed. Here, the velocity of the incoming flow is  $60 \text{ m/s}$  with the yaw angle of  $20^\circ$  which corresponds to the yaw angle at train speed  $v_t = 300 \text{ km/h}$  and crosswind speed  $v_w = 30 \text{ m/s}$ . According to the “Interim Measures for Management of Beijing–Tianjin Intercity Railway (2008)” in China, when the wind speed reaches above  $30 \text{ m/s}$ , the high-speed train should not run into the gale region. But here windbreak walls have been built along railways, so the train running at  $300 \text{ km/h}$  is highly safe when subjected to a crosswind of  $30 \text{ m/s}$ . Thus, the  $20^\circ$  yaw angle is used in the present study.

#### 3.1.1 3D Streamlines

The streamlines are always used to show the flow paths and vortex structures around the train. So in this section, to show the evident differences of 3D streamlines under different windbreak walls, an upstream line that is perpendicular to the ground was used as the launch start of the streamlines, see Fig. 5.

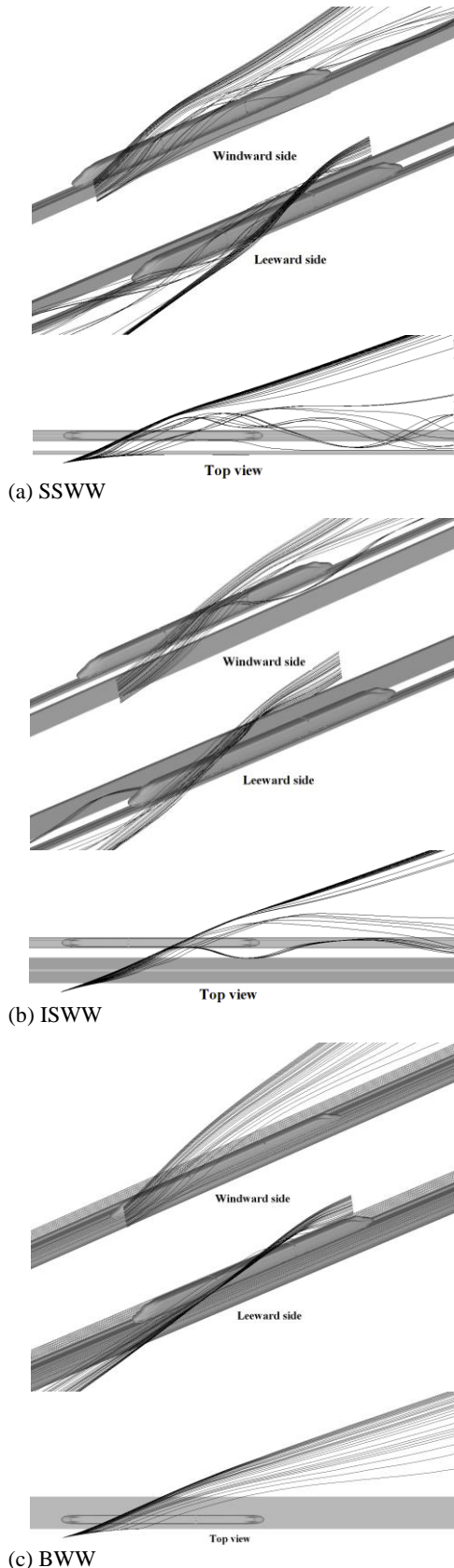


**Fig. 5. 3D streamlines around the train-windbreak wall. Windward side: flow is from left bottom to right top in these images. Leeward side: flow is from right top to left bottom in these images. Top view: flow is from left to right in these images.**

Since there are no holes (or 0% porosity) on the SSWW and ISWW, those streamlines are forced to flow over the wall and travel into the downstream region of the train. While for the BWW, 30% porosity allows parts of streamlines (i.e. flow) go through the wall and enter the region between the train and the wall. In the ISWW, some streamlines act on the train body after flowing over the wall, then flow into the tail vortex region along the train longitude direction. As to the SSWW, few streamlines can flow over the wall and then impact on the train. From the view of the displacement of the streamlines near ground, it is not difficult for the streamlines to flow over the ISWW, which shows almost equal possibility for the SSWW and BWW. Additionally, in the SSWW and ISWW, parts of streamlines that flow over the walls emerge into the wake regions, whereas in the BWW, due to the spatial location, the streamlines pass over the bridge and walls directly.

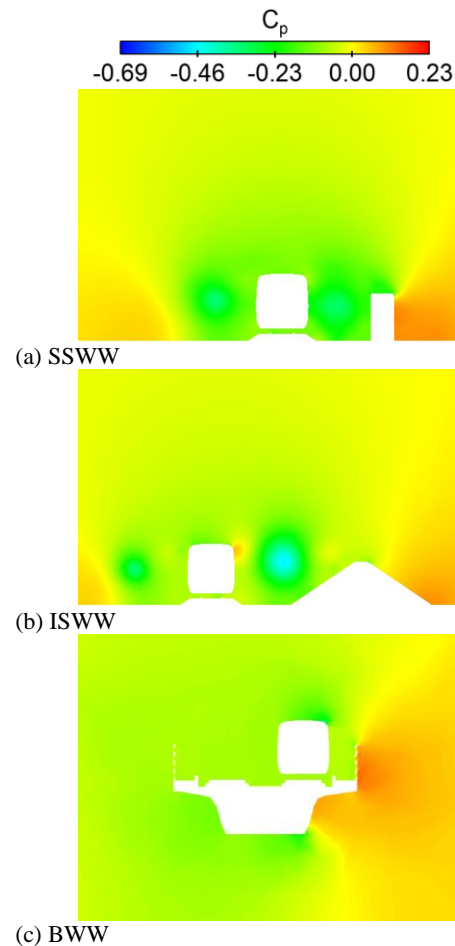


**Fig. 6. Pressure distributions around the train-windbreak wall. Flow is from right to left in these images.**

### 3.1.2 Pressure Distributions

Figure 6 shows the static pressure distributions around the train-windbreak walls in the middle cross-sectional plane of the middle car. On the windward side of the wall, there is positive pressure. Due to shielding effects, the train is in a

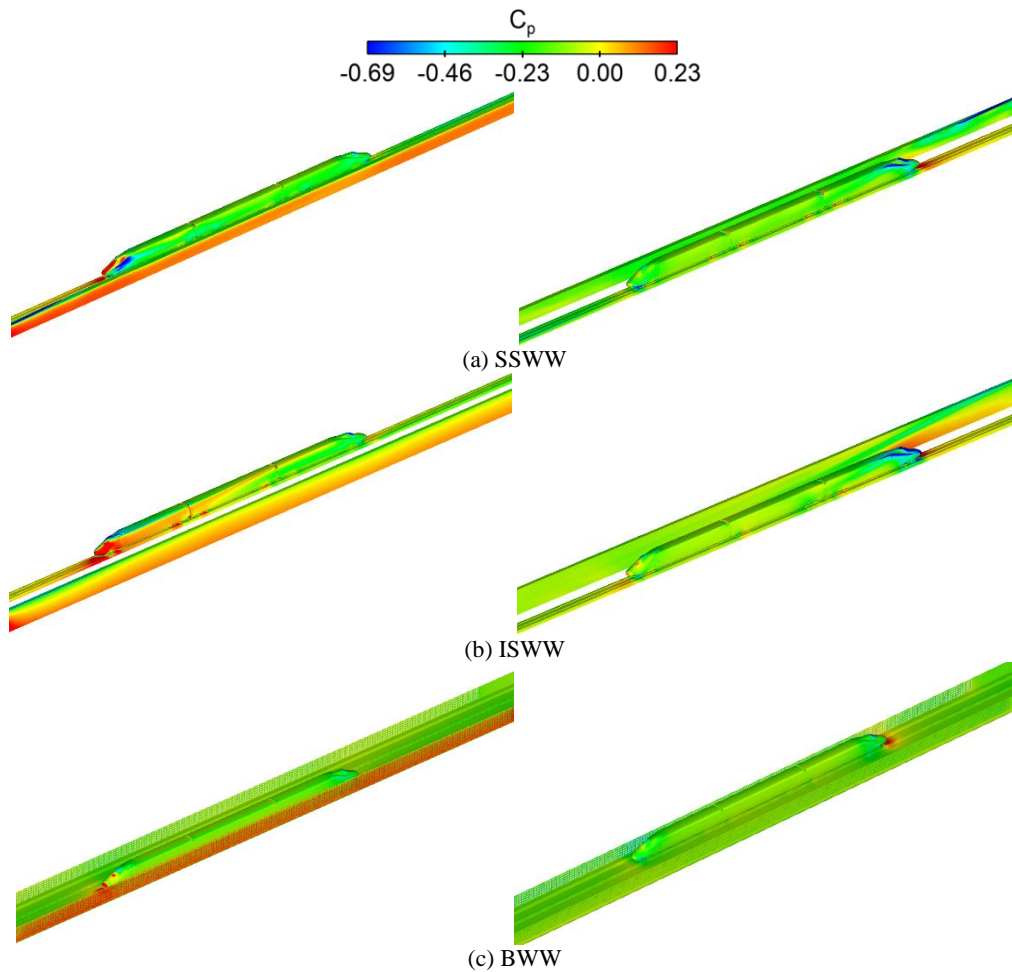


**Fig. 7. Pressure distribution of train-wind break wall surface subjected to different type windbreak walls. Left column: flow is from left bottom to right top in these images. Right column: flow is from right top to left bottom in these images.**

favourable windbreak performance environment (except of the ISWW where the windward side of the train shows a positive region) and a relatively balanced pressure environment around the train is formed, as reported in (Bocciolone *et al.*, 2008; Tomasini *et al.*, 2016; Zhang and Liu, 2012 and 2014; Zhang *et al.*, 2013 and 2017b). Since the BWW is located at a height above the ground, the positive pressure region is larger than those in the SSWW and ISWW. The negative pressure occurs locally in the leeward region of the wall and train in the SSWW and ISWW, while that shows the regions at the bottom, leeward side of the bridge, and the top of the train for the BWW.

Figure 7 shows the surface pressure on the train and walls. The windward side of the SSWW suffers the highest positive pressure, while the ISWW is the lowest. However, the pressure distributions on the train surface are opposite. The pressure on the streamlined head is affected by the complicated curved surface, which presents diversified distributions, while the pressure on the body with a uniform cross section shows more regular.

As shown in Fig. 7(a), in the SSWW, the positive pressure occurs locally on the front region of the

nose of the head car, while the strong negative pressure shows on the windward side of the streamlined head and slight negative pressure on the other side. Consequently, taking the pressure difference on the windward and leeward sides into account, the head car may suffer a side force that shows an inverse direction of the crosswind. The pressure on the leeward of the train is higher than that on the windward, so the negative side force could act on the middle and tail cars.

For the ISWW in Fig. 7(b), the entire windward of the head car, most of the windward of the middle car and small part of the arch region adjacent to the top of the tail car present positive pressure. This indicates after the airflow flows over the wall, it acts on the train body directly (see the 3D streamlines in Fig. 6(b)), resulting in a poor wind shielding effect for the train behind it, as reported in Zhang and Liu (2012 and 2014) and Zhang *et al.* (2017b). Besides, the strong negative pressure occurs on the leeward of the head car's nose, and the pressure on the leeward of the middle car is slight negative. According to the formation mechanism of the side force, this negative pressure will enhance the crosswind effect on the stability of the train.

A slight uniform negative pressure distribution on the train body is shown in Fig. 7(c) when the train is behind the BWW, corresponding to small side force. Similar to that pressure distribution on the streamlined head with complicated curved surfaces in the SSWW, the variation of the pressure is evident. As to the head car, due to the efficient windbreak effect of the BWW, the highest positive pressure turns up on the nose tip, which is similar to the pressure distribution on the nose of the train running in open air; slight negative pressure presents on its windward, corresponding to strong negative pressure on the leeward of the streamlined head. As a result, the head car probably suffers a larger positive side force. There is a larger region with stronger negative pressure on the windward of the tail car, indicating a negative side force.

According to this qualitative analysis, it is still hard to know how large the difference is on the windbreak effect in the three walls. Therefore, the pressure is plotted along a line on the train surface, as presented in Fig. 8. Line lies in the middle cross section of the middle car. For the SSWW, large pressure gradient is shown on the windward, leeward and top of the train surface; for the ISWW, this fast pressure change occurs on the upper part off the windward and top of the train body, while for the BWW, just on the top.

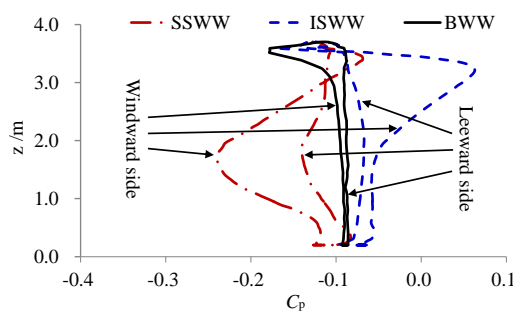


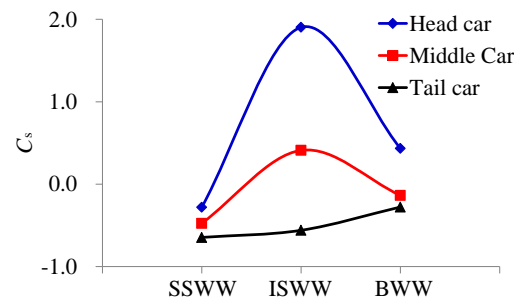
**Fig. 8. Pressure distributions on the cross section of the middle car subjected to different windbreak walls.**

When the train runs behind the SSWW, the pressure coefficient on the windward is smaller than on the leeward. The largest pressure difference occurs at approximate a half height of the train is -0.099. So the middle car is likely to have a negative side force. However, in the upper windward region close to the top, due to the effect of flow over the train, the pressure increases largely so as to be higher than that on the leeward. As a result, a shape of "8" is formed. Additionally, a small difference exists on the bottom and the top, contributing to a smaller lift force.

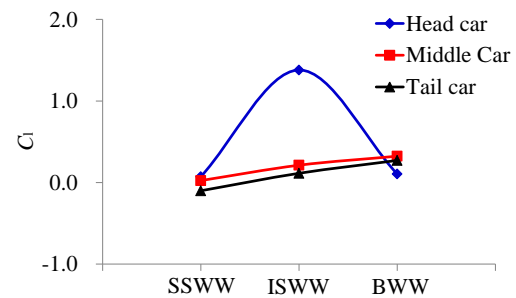
For the ISWW, it is clear that the pressure coefficient on the windward is larger than on the leeward, especially on the upper part of the windward. The largest positive pressure coefficient on the windward is up to 0.063, and the leeward negative pressure coefficient is -0.086 correspondingly, leading to the pressure difference of 0.149 which is 1.5 times of that in the SSWW. Therefore, the middle car will have a positive side

force. Since the pressure coefficient on the top is smaller than on the bottom, a positive lift force will act on the car.

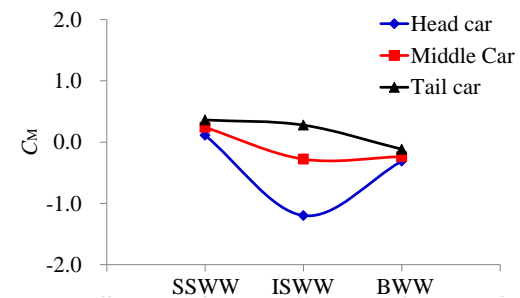
As to the BWW, the largest gradient of the pressure coefficient occurs on the top of the train. After that, the pressure goes to be approximately uniform on the windward and leeward, respectively. In addition, the pressure on the bottom is small, which undoubtedly leads to a larger lift force of the car. The pressure coefficient on the windward is lower than on the leeward, but the difference is small. Thus, the car will have a small negative side force, and its absolute value is the least.



(a) Side force coefficient



(b) Lift force coefficient



(c) Overturning moment coefficient

**Fig. 9. Aerodynamic coefficients of cars subjected to different windbreak walls.**

### 3.1.3 Aerodynamic Forces

Figure 9 shows the aerodynamic forces of the train behind different windbreak walls. As seen in Fig. 9(a), the side forces of the head, middle and tail cars are negative in the SSWW, indicating that the SSWW provides an efficient shielding effect and prevents large part of flow acting on the train. Additionally, due to the over-shielding protection, the side forces of the cars are negative. In the ISWW, the side force of the head car is larger, and

that of the middle car is also above zero, but the tail car has a negative side force, further indicating the poor shielding effect for the train. In the BWW, the side force of the head car is positive, while the middle and tail cars suffer small negative forces. On the whole, the train is in a favourable environment of side forces.

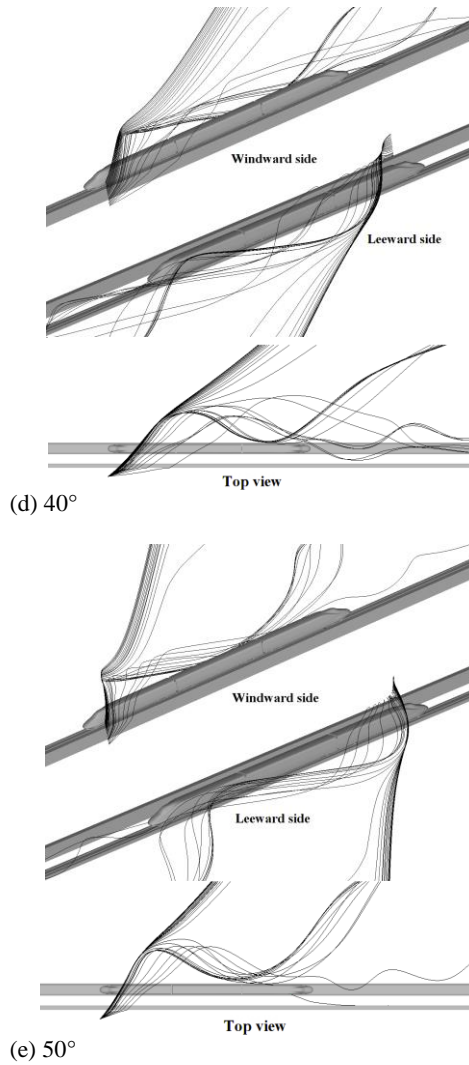
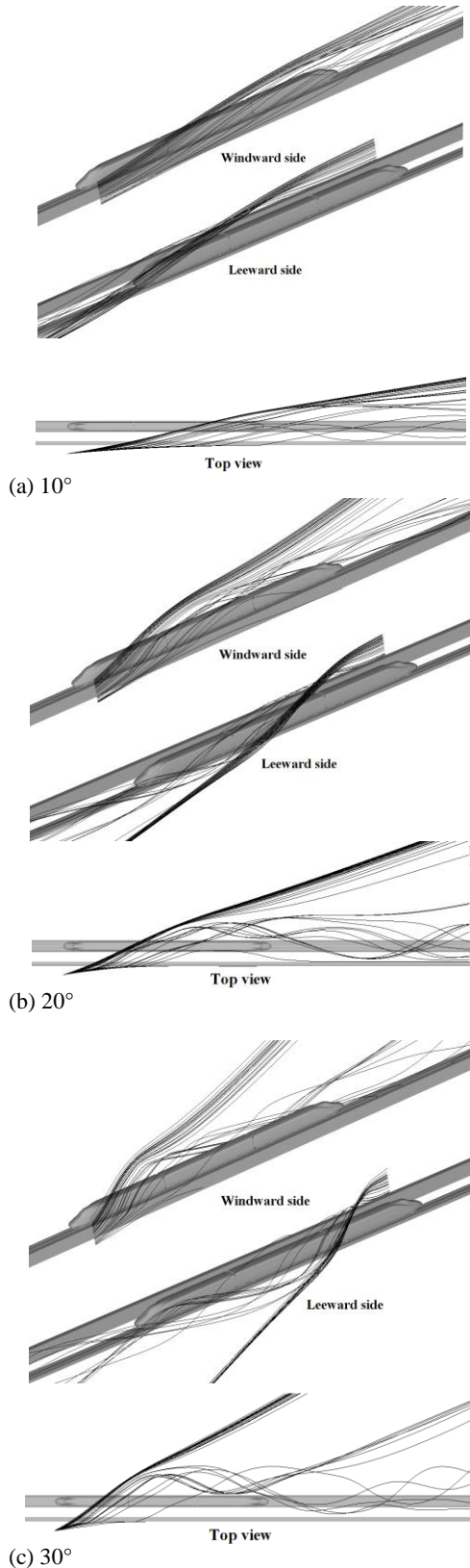


**Fig. 10. 3D streamlines around the train-windbreak wall in different yaw angles. Windward side: flow is from left bottom to right top in these images. Leeward side: flow is from right top to left bottom in these images. Top view: flow is from left to right in these images.**

As to the lift force in Fig. 9(b), in the SSWW, each car suffers a small positive or negative force, which can effectively reduce the floating status of the train. But in the ISWW, the larger lift force of the head car is prone to derailment of the train, while smaller ones of the middle and tail cars will be favourable. In the BWW, the force for each car is positive and small, and it is larger than the corresponding one in the SSWW.

Figure 9(c) shows the overturning moment coefficients. In the SSWW, all these are positive, while they are negative in the BWW. In both walls, the difference of the overturning moment coefficient between two cars is small, further showing they have favourable shielding effects. In the ISWW, so larger coefficient of the head car reduces the operational safety of the car. The coefficient of the middle car is negative and that of the tail car is positive.

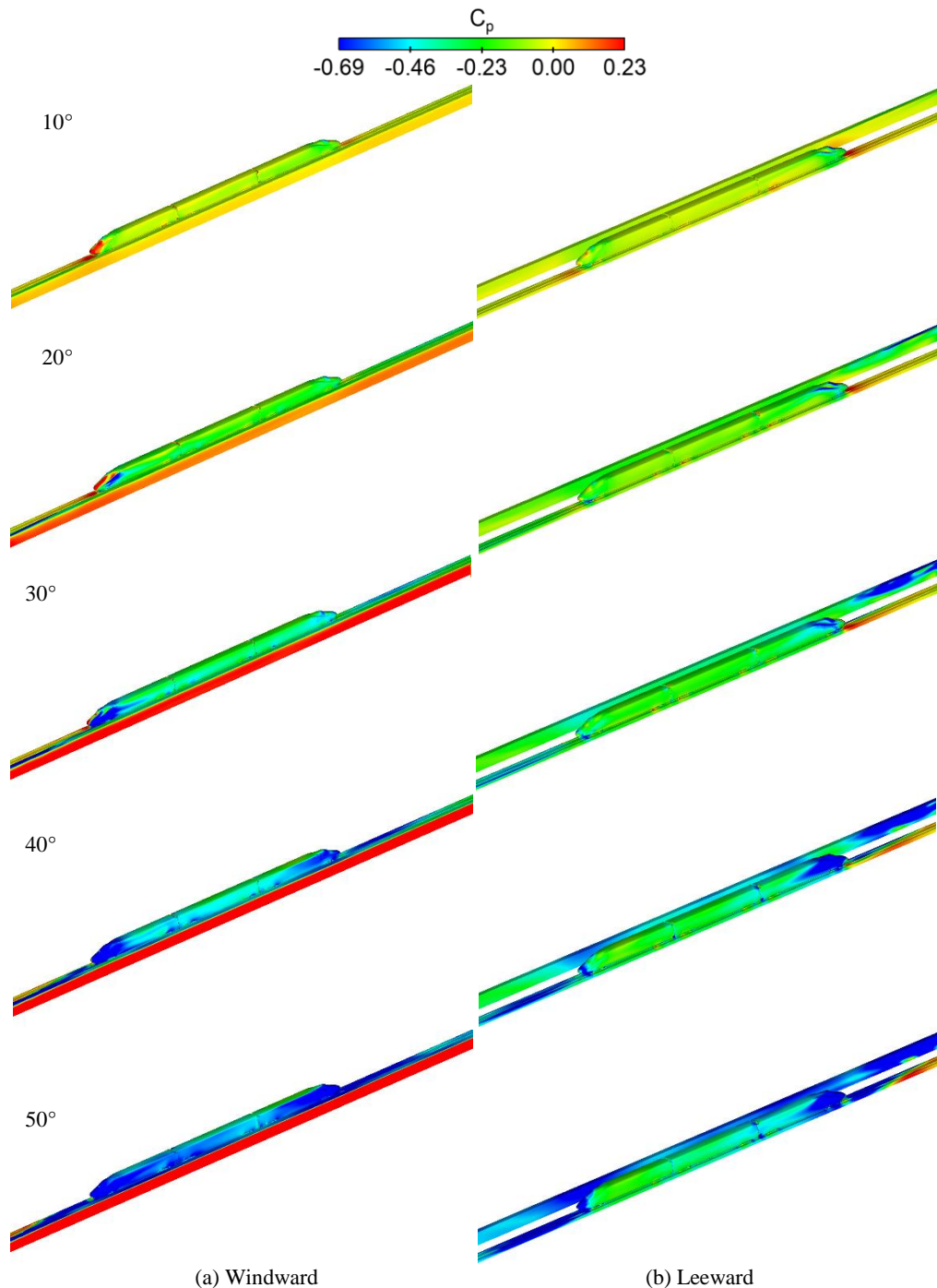


**Fig. 11.** Pressure distributions of train-wind break wall surfaces subjected to different yaw angles. Left column: flow is from left bottom to right top in these images. Right column: flow is from right top to left bottom in these images.

### 3.2 Yaw Angle

At an actual operational condition, due to complex wind and railway environments, the high-speed train always runs at different speeds. Therefore, various yaw angles can occur around the train. To understand the effects of yaw angles on the flow field around the train-windbreak wall, five yaw angles, i.e. 10°, 20°, 30°, 40° and 50°, were used. Here, the velocity of the incoming flow is 60 m/s, and the windbreak wall is the SSWW.

#### 3.2.1 3D Streamlines

Figure 10 shows the 3D streamlines around the train-windbreak wall in different yaw angles. The generation method of these streamlines is the same as that used in Section 3.1.1. This bunch of streamlines is divided into two parts, i.e. the upper is above the height of the wall and the lower is the rest. The upper part follows the yaw angle, flows over the top of the train along with low velocity streamlines from the other part; then part of it

emerges into the leeward space around the train-windbreak wall and finally into the wake region, while the other higher part flows along the yaw direction. The lower part is forced to climb along the wall. When it flows over the wall, a displacement along the train longitude direction has been found. Additionally, the yaw angle is smaller, the displacement of the streamlines close to the ground is larger. Since the velocity is slow, the probability of the streamlines converging to the trailing vortex region is large. The efficient shielding effect and complexity of wake vortices contribute to a more turbulent and complex wake region.

### 3.2.2 Pressure Distributions

Figure 11 shows the surface pressure on the train and walls. With the increase of yaw angles, the velocity component  $v$  in the  $y$  direction will increase, resulting in the pressure on the windward of the windbreak wall increases, while the pressures on the top and leeward of the wall, train surfaces show opposite trends due to the effective shielding performance of windbreak walls. At a small yaw angle, e.g.  $10^\circ$ , strong positive pressure is shown on the windward of the nose of the streamlined head. This indicates the flow over the wall can act on that part. In addition, small regions with positive pressure occur at the transitional arc part between the windward and the top of the train, the leeward of the train and the nose of the tail car. The positive pressure regions become smaller with the yaw angle increasing. When the yaw angle is  $40^\circ$ , the pressure around the train is basically negative. This negative pressure will be enhanced as the angle increases.

The pressure is plotted along a line on the train surface, as presented in Fig. 12. Line lies in the middle cross section of the middle car. The left curves show the pressure on the windward of the train, while the right ones correspond to the pressure on the leeward. The pressure difference of those on the windward and leeward of the train increases at a larger yaw angle, which contributes to high-pressure gradient on the transitional part close to the top or the bottom of the train. When the yaw angle is  $10^\circ$ , a region with small positive pressure occurs locally on the transitional arc that connects the windward and the top of the train. However, for the rest cases, the negative pressure is observed. When the yaw angle is small (e.g.  $10^\circ$  and  $20^\circ$ ), a point with equal pressure on the windward and leeward is found, leading to a shape of "8". This indicates that the windward of the train is affected by the flow that can flow towards the train body. After that, the flow rises due to the wall, and it cannot impact on the train body to increase the pressure. As a result, the pressure coefficient curve only presents a close loop. Those peak values of the pressure on the windward and leeward of the train exist at around half height of the train.

### 3.2.3 Aerodynamic Loads

The Aerodynamic coefficient of the train subjected to different yaw angles is shown in Fig. 13. In general, the absolute values of the train

aerodynamic coefficients increase at a higher yaw angle, indicating that the windbreak wall can protect the train against the crosswind condition.

In the case of  $10^\circ$  yaw angle, the side force coefficient of the head car is positive, the same as the crosswind flow, Fig. 13(a). As to the middle and tail cars, both are negative. This indicates the airflow impacts on the head car to a certain extent when it flows over the wall, whereas the shielding effect of the wall causes the negative side force coefficients of the middle and tail cars. With the increase of the yaw angle, the side force coefficients of each car decrease. However, there is a key point (i.e.  $30^\circ$ ) on the side force coefficient of the head car. Note that at  $30^\circ$  a larger difference of pressure on the windward side and leeward side of the head car is observed, as shown in Fig. 11, resulting in a large absolute side force. Under different yaw angle conditions, the force of the tail car is always larger than that of the middle car.

The lift force coefficients of the head car, middle car and tail car are small when the yaw angle is  $10^\circ$ , see Fig. 13(b). With the increase of yaw angles, the lift forces of the middle and tail cars invert from the positive to the negative, and the tail car shows a large absolute value.

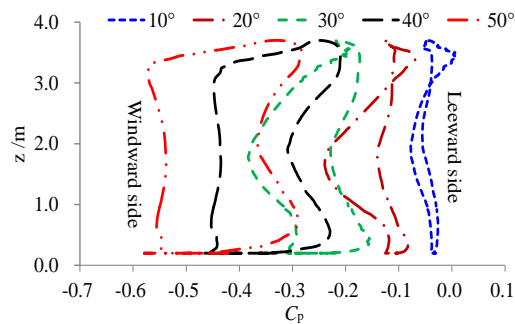


**Fig. 12. Pressure distributions on the cross section of the middle car subjected to different yaw angles.**

The overturning moments those are toward the windbreak wall at a higher yaw, except of the  $10^\circ$  yaw angle condition. The lift force coefficient curves are similar to the side force coefficient curves, which shows the side force has an impact the overturning moment. In different yaw cases, the moment of the tail car is the largest, while the least for the head car.

## 5. CONCLUSIONS

The steady SST  $k-\omega$  turbulence model was used to simulate that flow around the train-windbreak walls. The effects of different windbreak walls and yaw angles on the flow structures around the train-windbreak walls and the corresponding aerodynamic loads have been investigated. Based on the results and discuss, the study shows that:

- (1) Efficient windbreak wall structures could transfer the positive pressure on the train's windward to the wall's, then the airflow can not

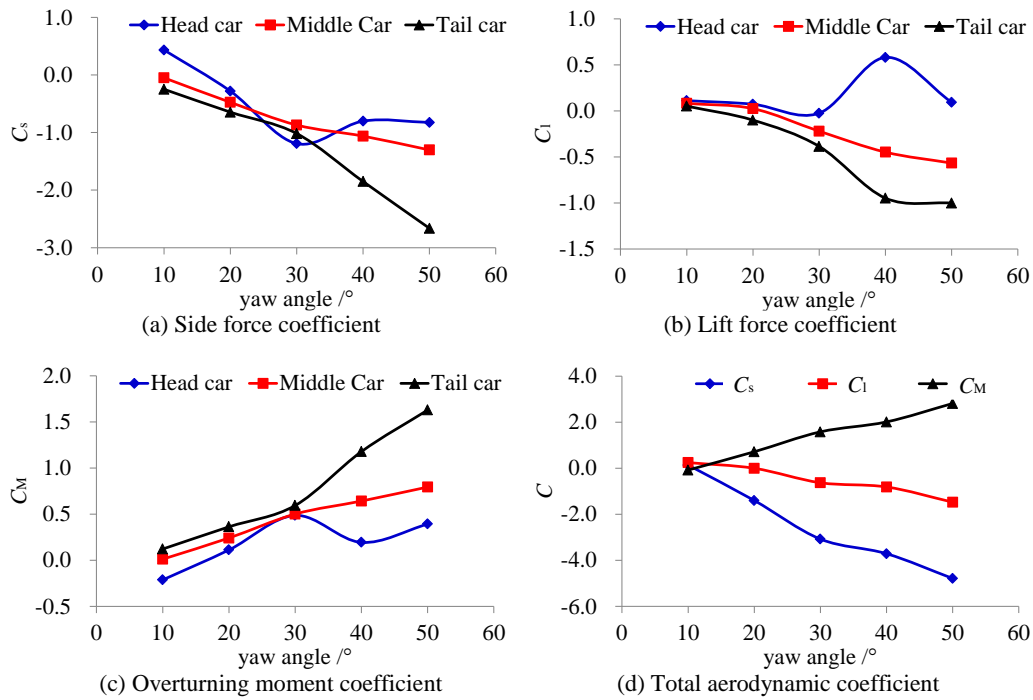


Fig. 13. Aerodynamic coefficients of cars subjected to different yaw angles.

directly act on the train body, so that the train is basically in a favourable negative pressure environment. Except of the streamlined head, the pressure distribution of the train body is basically uniform, and the pressure on the leeward of the train is a little larger than on the windward.

- (2) As to the ISWW, the airflow flows over the wall easily and acts on the train directly, leading to a larger side force, which indicates that the ISWW has a poor shielding effect for the train. While in the SSWW and BWW, the streamlines are mostly forced to flow upward, and couldn't act on the train generally. The pressure distribution of the train body is uniform, and the train is basically in a negative pressure environment. Therefore, small loads are found on the train, which shows efficient anti-wind performance.
- (3) A larger yaw angle leads to a larger speed of the wind, therefore, higher pressure is observed on the windward of the windbreak wall. At a small yaw angle, e.g. 10°, strong positive pressure is shown on the windward of the nose of the streamlined head. This indicates the flow over the wall can act on that part. The positive pressure regions become smaller with the yaw angle increasing. When the yaw angle is 40°, the pressure around the train is basically negative. This negative pressure will be enhanced as the angle increases.
- (4) The pressure difference of those on the windward and leeward of the train increases at a larger yaw angle, which contributes to high-pressure gradient on the transitional part close to the top or the bottom of the train. When the yaw angle is small (e.g. 10° and 20°), a point

with equal pressure on the windward and leeward is found, leading to a shape of "8". After that, the flow rises due to the wall, and it cannot impact on the train body to increase the pressure. As a result, the pressure coefficient curve only presents a close loop. Those peak values of the pressure on the windward and leeward of the train exist at around half height of the train.

- (5) With the increase of the yaw angle, the absolute values of the train aerodynamic coefficients increase gradually, and the tail car's is the largest at a larger angle (>30°), indicating an over-shielding effect for the train. Thus, when designing the windbreak walls, yaw angles should be taken into account.

#### ACKNOWLEDGEMENTS

The authors acknowledge the computing resources provided by the High-speed Train Research Center of Central South University, China.

The research described in this paper was supported by the National Railway Administration of China (Grant No. KF2017-006), the National key R & D program of China (Grant No. 2016YFB1200506-03), the Technology Research and Development Program of China Railway Corporation (Grant No. 2017J010-B) and the National Natural Science Foundation of China (Grant Nos. U1534210 and 51605044).

#### REFERENCES

Avadiar, T., J. Bell, D. Burton, H. Cormaty and C.

- Li (2016). Analysis of high-speed train flow structures under crosswind. *Journal of Mechanical Science and Technology* 30, 3985-3991.
- Avila-Sanchez, S., O. Lopez-Garcia, A. Cuerva and J. Meseguer (2016). Characterisation of cross-flow above a railway bridge equipped with solid windbreaks. *Engineering Structures* 126, 133-146.
- Baker, C. J. (1999). The wind tunnel determination of crosswind forces and moments on a High Speed Train. *Proceedings of the TRANSAERO Symposium*, May 04-05, 1999, Paris, France.
- Bocciolone, M., F. Cheli, R. Corradi, S. Muggiasca and G. Tomasini (2008). Crosswind action on rail vehicles: Wind tunnel experimental analyses. *Journal of Wind Engineering and Industrial Aerodynamics* 96, 584-610.
- Cheli, F., F. Ripamonti, D. Rocchi and G. Tomasini (2010). Aerodynamic behaviour investigation of the new EMUV250 train to cross wind. *Journal of Wind Engineering and Industrial Aerodynamics* 98(4/5), 189-201.
- Chen, Z., T. Liu, Z. Jiang, Z. Guo and J. Zhang (2018). Comparative analysis of the effect of different nose lengths on train aerodynamic performance under crosswind. *Journal of Fluids and Structures* 78, 69-85.
- Fujii, T., T. Maeda, H. Ishida, T. Imai, K. Tanemoto and M. Suzuki (1999). Wind-Induced Accidents of Train/Vehicles and Their Measures in Japan. *Quarterly Report of Railway Technical Research Institute* 40(1), 50-55.
- Gao, G., J. Zhang and X. Xiong (2014). Location of anemometer along Lanzhou-Xinjiang railway. *Journal of Central South University* 21(9), 3698-3704.
- Ge, S. C. and F. Q. Jiang (2009). Analyses of the Causes for Wind Disaster in Strong Wind Area along Lanzhou-Xinjiang Railway and the Effect of Windbreak. *Journal of railway engineering society* 5, 1-4. (in Chinese)
- Gong, J. and P. Wang (2012). Research on Gale Monitoring & Early Warning System of High-speed Railway. *High Speed Railway Technology* 3(1), 5-8, 14.
- Hemida, H. and S. Krajnovic (2010). LES study of the influence of the nose shape and yaw angles on flow structures around trains. *Journal of Wind Engineering and Industrial Aerodynamics* 98(1), 34-46.
- Khier, W., M. Breuer and F. Durst (2000). Flow structure around trains under side wind conditions: a numerical study. *Computers and Fluids* 29, 179-195.
- Liu, H., H. Q. Tian and Y. F. Li (2009). Short term forecasting optimization algorithms for wind speed along QinghaiTibet railway based on different intelligent modeling theories. *Journal of Central South University* 16(4), 690-696.
- Liu, T. and J. Zhang (2013). Effect of landform on aerodynamic performance of high-speed trains in cutting under cross wind. *Journal of Central South University* 20, 830-836.
- Peters, J (2004). How to Reduce the Cross Wind Sensitivity of Trains. McCallen, R., Browand, F., and Ross, J.. *The Aerodynamics of Heavy Vehicles: Trucks, Buses, and Trains*. New York, Springer-Verlag 453-467.
- Rezvani, M. A. and M. Mohebbi (2014) Numerical calculations of aerodynamic performance for ATM train at crosswind conditions. *Wind and Structures* 18, 529-548.
- Rolén, C., T. Rung and D. Wu (2004). Computational modelling of cross-wind stability of high-speed trains. *Proc. European Congress on Computational Methods in Applied Sciences and Engineering*. Jyväskylä, 24-28 July 2004.
- Sima, M., S. Eichinger, A. Blanco and I. Ali (2015) Computational fluid dynamics simulation of rail vehicles in crosswind: Application in norms and standards. *Proceedings of the Institution of Mechanical Engineers Part F- Journal of Rail and Rapid Transit* 229, 635-643.
- Suzuki, M., K. Tanemoto and T. Maeda (2003). Aerodynamic characteristics of train/vehicles under cross winds. *Journal of Wind Engineering & Industrial Aerodynamics* 91, 209-218.
- Tomasini, G., S. Giappino, F. Cheli and P. Schito (2016). Windbreaks for railway lines: Wind tunnel experimental tests. *Proceedings of the Institution of Mechanical Engineers, Part F: Journal of Rail and Rapid Transit* 230(4), 1270-1282.
- Wetzel, C. and C. Proppe (2007). Probabilistic Assessment of the Crosswind Stability of Railway Vehicles. *Proceedings of Weimar Optimization and Stochastic Days* 4.0, Weimar, 2007.
- Wikipedia (2015). List of wind-related railway accident. [https://en.wikipedia.org/wiki/List\\_of\\_wind-related\\_railway\\_accidents](https://en.wikipedia.org/wiki/List_of_wind-related_railway_accidents), 2015-8-29.
- Yao, S. B., D. L. Guo, Z. X. Sun, G. W. Yang and D. W. Chen (2014). Optimization design for aerodynamic elements of high speed trains. *Computers and Fluids* 95, 56-73.
- Zhang, J. and T. H. Liu (2012). Optimization Research on the Slope Angle of the Earth Type Windbreak Wall of Xinjiang Single-Track Railway. *China Railway Science* 33(2), 28-32.
- Zhang, J. and T. H. Liu (2014). Multistep design of earth type windbreak wall along Lanzhou-Xinjiang railway. *Journal of Central South*

- University: Science and Technology* 45(4), 1334-1340.
- Zhang, J., G. Gao, T. Liu and Z. Li (2017b). Shape Optimization of a Kind of Earth Embankment Type Windbreak Wall along the Lanzhou-Xinjiang Railway. *Journal of Applied Fluid Mechanics* 10(4), 1189-1200.
- Zhang, J., G. Gao, X. Xiong, T. Liu and F. Liu (2016). Influence of types of steel poles on measurements by wind speed sensors along high-speed railways. *Journal of Applied Fluid Mechanics* 9(1): 243-251.
- Zhang, J., G. J. Gao and L. J. Li (2013). Height optimization of windbreak wall with holes on high-speed railway bridge. *Journal of Traffic and Transportation Engineering* 13(6), 28-35.
- Zhang, J., G. J. Gao, S. Huang and T. H. Liu (2015a). Effect on measurements of anemometers due to a passing high-speed train. *Wind and Structures* 20(4), 549-564.
- Zhang, J., G. J. Gao, T. H. Liu and Z. W. Li (2015b) Crosswind stability of high-speed trains in special cuts. *Journal of Central South University* 22, 2849-2856.
- Zhang, J., K. He, X. Xiong, J. Wang and G. Gao (2017a). Numerical Simulation with a DES Approach for a High-Speed Train Subjected to the Crosswind. *Journal of Applied Fluid Mechanics* 10(5), 1329-1342.
- Zhang, J., X. Liang, T. Liu and L. Lu (2011). Optimization research on aerodynamic shape of passenger car body with strong crosswind. *Journal of Central South University: Science and Technology* 42(11), 3578-3584.